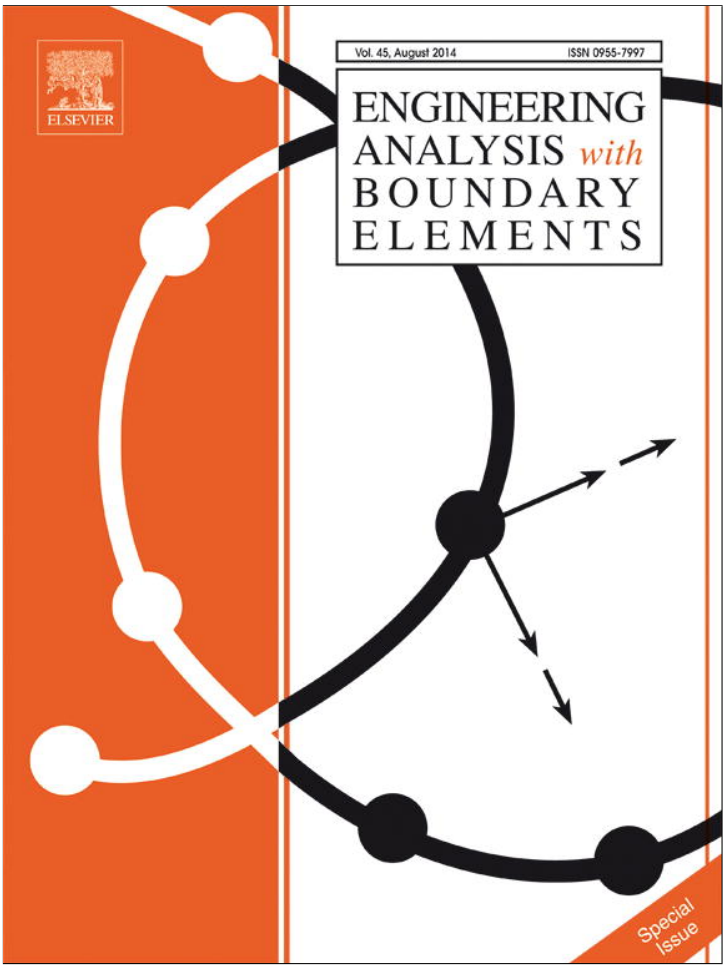

Engineering Analysis with Boundary Elements 45 (2014) 20–28

Contents lists available at ScienceDirect

Engineering Analysis with Boundary Elements

journal homepage: www.elsevier.com/locate/enganabound

Coupled BEM–FEM analysis of flow and heat transfer over a solar thermal collector

J. Ravnik *, M. Hriberšek, L. Škerget

Faculty of Mechanical Engineering, University of Maribor, Smetanova 17,SI-2000 Maribor, Slovenia

ARTICLE INFO

Article history:
Received 9 June 2011
Accepted 20 December 2012
Available online 21 February 2014

Keywords:
Solar thermal collector
Boundary element method
Fluid flow
Heat transfer
Velocity–vorticity
Large Eddy Simulation

ABSTRACT

A wavelet transform based BEM numerical scheme is used for Large Eddy Simulation of turbulent natural and forced convection of air flowing over a solar thermal collector. The collector is enclosed by vertical fins forming an open shallow cavity. The numerical scheme employs the velocity–vorticity formulation of Navier–Stokes equations using LES turbulence model where boundary element and finite element methods are combined. Grids with up to 2×10^5 nodes are used in simulations lasting for 6×10^4 time steps. Three inflow air velocities are considered corresponding to Reynolds number value up to 2×10^4. Temperature difference between air and collector of about 50 K is considered. Heat transfer from the thermal solar collector is studied via the average Nusselt number value, its time series and its relationship to the values of Reynolds and Rayleigh numbers. The results show that the largest heat losses occur behind the fin due to shedding of large vortices that transport hot air away from the collector. Heat losses decrease along the central part of the collector and feature another smaller peak just before the air hits the fin on the opposite side of the collector.

1. Introduction

Recent developments in the area of advanced engineering analysis are mainly connected with development of novel computational tools, based on numerical solution of complex physical phenomena. Turbulent fluid flow with heat transfer is a typical example of a problem, where the use of classical engineering approaches in form of scale-up assumptions and resulting empirical models fall short when encountering complex heat transfer geometries. Whereas empirical correlations are developed mainly for simple geometries, such as a flat plate or a cylinder, even a slight perturbation to such a geometry puts the applicability of the empirical correlation, for example for the Nusselt number, under question. The same holds when characteristic velocity field should be determined in a form of a single velocity value, an example when forced convection is under investigation. Such a relatively simple example is flow over a cavity, where a cavity could be described as a flat plate bounded by two finite vertical walls.

Flows over cavities are encountered in many engineering applications. Flows over solar thermal collectors [1–4] and flow in street canyons [5] are only two of many such examples. Solar thermal collectors enclosed by vertical fins form an open shallow cavity capturing hot air above the collector and thus reducing heat transfer.

Several studies dealing with flow and heat transfer in and over an open shallow cavity are available in the literature. Research started with cavities of aspect ratio (height of the wall versus width of the cavity) of one [6,7]. Chan and Tien [8] continued their research on open shallow cavities. Bilgen [9] studied natural convection, radiation and conduction heat transfer in a shallow cavity configuration of a passive solar massive wall systems with fins attached to the heated surface.

Gomes [1] performed experiments on flows over solar thermal collectors to show that heat transfer can be significantly altered, when the collector is enclosed into a cavity. The same problem was numerically studied by Zdanski and co-workers [2–4]. Even though the flow over a solar thermal collector is always three-dimensional, Zdanski used a 2D approximation. Such an approximation is used in this paper as well.

Mesalhy et al. [10] studied the flow over a shallow cavity heated with constant heat flux from the bottom side both experimentally and numerically. In the numerical simulation the standard k–ϵ turbulence model was used to account for the turbulent fluctuations. Variations of cavity aspect ratio and Reynolds number have been studied. They reported that a single elongated eddy has been formed for aspect ratio lower than 7.

* Corresponding author.
E-mail addresses: jure.ravnik@uni-mb.si (J. Ravnik), matjaz.hribersek@uni-mb.si (M. Hriberšek), leo@uni-mb.si (L. Škerget).

http://dx.doi.org/10.1016/j.enganabound.2014.01.018
0955-7997

As the aspect ratio increases the flow impinges with the cavity floor creating two eddies, one beside the upstream cavity side and the second beside the downstream cavity side.

Polat and Bilgen [11] numerically examined conjugate heat transfer in inclined open shallow cavities. A thick wall facing the opening was heated by a constant heat flux, sides perpendicular to the heated wall were insulated and the opening was in contact with a fluid at constant temperature and pressure. Conjugate heat transfer by conduction and natural convection was studied by numerically solving equations of mass, momentum and energy. They reported that heat transfer is an increasing function of the aspect ratio up to a critical Rayleigh number above which the relationship changes and it becomes a decreasing function of aspect ratio.

Recently, Alloui and Vasseura [12,13] studied flow and heat transfer of nanofluids and micropolar fluids in shallow cavities. The critical Rayleigh number for the onset of supercritical convection of nanofluids is predicted explicitly. Analytical studies are compared with numerical experiments.

Most available studies use either a laminar setting or employ a Reynolds averaged Navier Stokes equations (RANS) approach to turbulence modelling. Due to the known RANS limitations when flows with adverse pressure gradients are encountered and recirculation regions are an important part of the flow field, we decided to use the Large Eddy Simulation approach for solving turbulent flow over an open cavity, where accurate predictions of recirculating flow regions are of main importance for correct computation of heat transfer phenomena. Salat et al. [14] compared the results of modelling turbulent natural convection at high Rayleigh number value between experimental data, 2D LES, 2D DNS and 3D LES computations. They reported that only minor differences are observed between the 2D and 3D results and concluded that a 2D calculation could be used as a first approximation for general flow structure in cavities at Rayleigh number value about 10^{10}. Peng and Davidson [15] performed a LES study of turbulent buoyant flow in a $1:1$ enclosure at $Ra=1.59\times10^9$ using a dynamic Smagorinsky model as well as the classical Smagorinsky model with Van Driest damping.

In the present work both forced and natural convection in a flow over a shallow cavity were studied. The shallow cavity was used as a model of a solar thermal collector, composed of the flat floor and two side walls (fins). Heat transfer within the cavity was studied for the incoming air flowing parallel to the cavity floor.

The planar Large Eddy Simulation (LES) is used with the velocity–vorticity formulation of the incompressible Navier–Stokes equations. The velocity–vorticity formulation of the Navier–Stokes equations in combination with the boundary element method is a promising concept for numerical solution of fluid flow problems. Solution of the flow kinematics equation is obtained by the boundary element method (BEM) and provides boundary vorticity values, leading to a well posed vorticity transport equation. It is written in a form directly applicable for the first kind boundary value problems. Velocity–vorticity LES has been investigated by Tenaud et al. [16] and Mansfield et al. [17], each using a different solution technique for computation of boundary vorticity values. We propose to use BEM because of its unique advantage for solving the boundary vorticity values directly.

For the solution of the domain values Škerget et al. [18] and Ramšak and Škerget [19] proposed a subdomain BEM technique. Although the subdomain technique results in sparse matrices, it still requires a considerable amount of computer memory and CPU time. These requirements were reduced by Žunič et al. [20] who proposed using FEM for the solution of the domain and was able to simulate 2D laminar flows in velocity–vorticity formulation. In order to be able to perform a LES simulation, a wavelet compression algorithm is introduced on fully populated matrices, resulting from the BEM calculation of boundary vorticity, to further decrease the computer memory and CPU time requirements of the coupled BEM–FEM algorithm. A discrete wavelet transform for vectors of arbitrary length, developed by Ravnik et al. [21] as well as the BEM–FEM coupling algorithm developed by Ravnik et al. [22], was used.

2. Velocity–vorticity based Large Eddy Simulation

In this work we assume an incompressible viscous Newtonian fluid with constant material properties: density ρ, viscosity ν and thermal diffusivity $\alpha=\lambda/\rho c_p$. The continuity equation (mass conservation law) within this approximation, $\vec{\nabla}\cdot\vec{v}=0$, requires the velocity field $\vec{v}$ to be solenoidal, i.e. divergence free. In order to write the Navier–Stokes equations buoyancy is modelled within the Boussinesq approximation. Density variations with temperature $\rho(T)=\rho_0[1-\beta_T(T-T_0])$ are considered only in the buoyancy term and defined by the thermal volume expansion coefficient β_T and the temperature difference.

The well established [23,24] LES approach is to filter the equations of continuity, momentum and heat transport and rewrite them in a form, having the same terms as the original equation with an additional term, describing the difference between the two equations, i.e. the dissipation effects. However, we will use velocity–vorticity based LES, where the vorticity transfer equation is filtered instead of the momentum transfer equation. Similar to Richardson's energy cascade, Taylor's [25] vorticity transfer hypothesis also proposes transfer of vorticity from the large scales towards the small scales and its dissipation by the small scales.

In this work, we employ the velocity–vorticity formulation of the Navier–Stokes equations. Vorticity $\vec{\omega}$ is defined as the curl of the velocity $\vec{\omega}=\vec{\nabla}\times\vec{v}$. In this formulation the continuity equation is used to transform the vorticity definition into a kinematics equation:

$$\nabla^2\vec{v}+\vec{\nabla}\times\vec{\omega}=0, \tag{1}$$

which relates the velocity and vorticity fields for every point in space and time. Both the vorticity and velocity fields must be solenoidal, in order for this equation to be fulfilled.

Similarly, the momentum conservation equation is replaced by the vorticity transport equation:

$$\frac{\partial\vec{\omega}}{\partial t}-\vec{\nabla}\times(\vec{v}\times\vec{\omega})=-\frac{Ra}{PrRe^2}\vec{\nabla}\times T\vec{g}-\frac{1}{Re}\vec{\nabla}\times\vec{\nabla}\times\vec{\omega}. \tag{2}$$

The non-dimensional form of equations is used. Here $Re=v_0h/\nu$ is the Reynolds number, $Pr=\nu\rho c_p/\lambda$ is the Prandtl number and $Ra=g\beta_T\Delta Th^3/\nu\alpha$ is the Rayleigh number. The form of vorticity transfer equation (2) is appropriate for LES filtering. The application of the filter to Eq. (2) filters all field functions in linear terms. Special consideration is needed for the nonlinear term $\vec{\nabla}\times(\vec{v}\times\vec{\omega})$, which requires an introduction of a residual vorticity vector $\vec{\tau}^{\omega}$ that represents the difference of a filtered product and a product of filtered quantities $\vec{\tau}^{\omega}=\overline{\vec{v}\times\vec{\omega}}-\overline{\vec{v}}\times\overline{\vec{\omega}}$. The filtered equation (2) reads as

$$\frac{\partial\vec{\omega}}{\partial t}-\vec{\nabla}\times(\vec{v}\times\vec{\omega})=-\frac{Ra}{PrRe^2}\vec{\nabla}\times T\vec{g}-\frac{1}{Re}\vec{\nabla}\times\vec{\nabla}\times\vec{\omega}+\vec{\nabla}\times\vec{\tau}^{\omega}, \tag{3}$$

where we have, due to clarity of notation, omitted the bars indicating that all field functions have been filtered. By comparing non-filtered equation (2) with the filtered equation (3) we see that the difference is only in the residual vorticity vector term $\vec{\nabla}\times\vec{\tau}^{\omega}$.

Thus the residual vorticity vector $\vec{\tau}^{\omega}$ represents the dissipation of vorticity by the small scales according to the turbulent vorticity transfer theory of Taylor [25].

The filtered form of the energy conservation law, i.e. the heat transport equation is

$$\frac{\partial T}{\partial t}+(\vec{v}\cdot\vec{\nabla})T=\frac{1}{RePr}\nabla^2 T-\vec{\nabla}\cdot\vec{\tau}^{h}, \tag{4}$$

where the residual temperature vector $\vec{\tau}^{h}$ is defined as the difference between the filtered product of temperature and velocity field minus the product of filtered fields $\vec{\tau}^{h}=\overline{T\vec{v}}-\overline{T}\,\overline{\vec{v}}$.

Numerous LES studies used the Smagorinsky [26] and vorticity based [17] models for modelling the dissipative effect of subgrid scales. Both types of models model the contribution of subgrid scales via the turbulent viscosity hypothesis. We are modelling the subgrid scales with analogy to molecular transfer of kinetic energy to heat; the process which is defined by viscosity. The residual heat vector is modelled using the gradient hypothesis. Here we are introducing a non-dimensional subgrid scale viscosity ν_{sgs} and subgrid diffusivity α_{sgs} by

$$\vec{\tau}^{\omega}=-\nu_{sgs}\vec{\nabla}\times\vec{\omega},\quad \vec{\tau}^{h}=-\alpha_{sgs}\vec{\nabla}T. \tag{5}$$

Using the residual vorticity vector (5) and after doing some algebraic manipulations, we arrive at the final form of the filtered vorticity transport equation. In this paper the solution of the vorticity – – velocity based LES was obtained in planar geometry. In planar geometry the kinematics equation (1) connects the velocity components v_x, v_y to the scalar vorticity field ω; $\vec{\omega}=(0,0,\omega)$. Pointing gravity in the negative y direction, the filtered vorticity transport equation can be written as

$$\frac{\partial\omega}{\partial t}+(\vec{v}\cdot\vec{\nabla})\omega=\left(\frac{1}{Re}+\nu_{sgs}\right)\nabla^2\omega-\frac{Ra}{PrRe^2}\frac{\partial T}{\partial x}+\vec{\nabla}\omega\cdot\vec{\nabla}\nu_{sgs}. \tag{6}$$

Inserting the residual heat vector (5) into diffusion advection equation for temperature (4) we obtain

$$\frac{\partial T}{\partial t}+(\vec{v}\cdot\vec{\nabla})T=\left(\frac{1}{RePr}+\alpha_{sgs}\right)\nabla^2 T+\vec{\nabla}T\cdot\vec{\nabla}\alpha_{sgs} \tag{7}$$

Several models for the subgrid scale viscosity have been proposed. For vorticity transport equation (6) the enstrophy based model given by Mansour [27,28] was used: $\nu_{sgs}=(C\Delta)^2\sqrt{\vec{\omega}\cdot\vec{\omega}}$. A sharp spectral filter is used; thus the filter width equals $\Delta=(\Delta_x\Delta_y)^{1/2}$. It is known [29] that turbulent oscillations die out in the vicinity of walls. Therefore, the residual vorticity vector (5) must also limit to zero when approaching a solid wall. Damping of the filter width is used to achieve zero residual tensor and vector at the wall [29]. We employed Van Driest type damping d_{vd} to bring the subgrid scale viscosity to zero in the vicinity of solid walls:

$$d_{vd}=1-e^{[-y^+/25]};\quad \nu_{sgs}=(C\Delta d_{vd})^2\sqrt{\vec{\omega}\cdot\vec{\omega}}. \tag{8}$$

On the basis of experimental observations the turbulent viscosity of isotropic turbulence was found to be comparable with the turbulent diffusivity for the complete turbulent spectrum, their relationship being close to linear:

$$\alpha_{sgs}=\frac{1}{Pr_t}\nu_{sgs}, \tag{9}$$

where Pr_t is the empirically defined turbulent Prandtl number.

3. Coupled wavelet BEM – – FEM solution algorithm

The solution of the vorticity – – velocity based LES was obtained in planar geometry. In planar geometry the kinematics equation (1) connects the velocity components v_x, v_y to the scalar vorticity field ω. Our complete system of equations is thus made of two scalar Poisson type kinematic equations for both velocity component equations (1) and of the diffusion advection equations for temperature (7) and vorticity (6). Having the Dirichlet type velocity boundary conditions on all walls, the wavelet based boundary element method is used to calculate boundary vorticity [21]. The following integral form of the kinematics equation is used

$$c(\xi)\vec{v}(\xi)+\int_\Gamma\vec{v}(\vec{n}\cdot\vec{\nabla})u^\star\,d\Gamma = \int_\Gamma\vec{v}\times(\vec{n}\times\vec{\nabla})u^\star\,d\Gamma+\int_\Omega(\vec{\omega}\times\vec{\nabla}u^\star)\,d\Omega, \tag{10}$$

where $u^\star$ is the fundamental solution of the Laplace equation ($u^\star=(1/2\pi)\ln(1/r)$ in 2D), $\vec{n}$ is the unit normal, ξ is the source point and $c(\xi)$ is the geometrical factor.

With the boundary vorticity values as the unknowns, the discrete (matrix – vector) form of equation (10) is [22]

$$[D^\Gamma]\{\omega^\Gamma\}=([C]+[H])\{v_t\}+[H^t]\{v_n\}-[D^{\Omega\setminus\Gamma}]\{\omega^{\Omega\setminus\Gamma}\}. \tag{11}$$

The matrices are fully populated and unsymmetrical. Storage and algebraic operation with these matrices requires large amount of onboard memory and CPU time. To tackle this problem we employed a wavelet transform technique for rectangular matrices developed by Ravnik et al. [21]. Wavelet transform of all rows and columns of matrices is calculated and afterwards small matrix elements may be neglected. Thus, a sparse matrix is obtained and the boundary vorticity values may be calculated efficiently.

After the calculation of the boundary vorticity values the kinematic equations (1) are solved again for domain velocities. Explicit BEM or FEM can be used. With the new velocity field the temperature transport equation (7) is solved to obtain a new temperature field. Finally, the vorticity transport equation (6) is solved using the new boundary vorticity, domain velocities and temperatures. Both transport equations are solved by FEM. The procedure is repeated until convergence criteria is fulfilled (RMS difference between vorticity fields in subsequent iterations is used).

Both the vorticity transport equation (6) and temperature transport equations (7) are of the diffusion – – advection type. Here we describe a FEM solution of a general form of equations. Let the unknown scalar field function (vorticity or temperature) be denoted by u. First of all the partial time derivative has to be approximated by the following second order approximation

$$\frac{\partial u}{\partial t}\approx\frac{3u-4u^n+u^{n-1}}{2\Delta t}, \tag{12}$$

where u is the field function to be calculated in the next time step, u^n is the field function in the present time step, and u^{n-1} is the previous time step field function. The time step size is Δt. Having the approximation of the time derivative in mind, one can state the general diffusion advection equation in the form

$$\beta u+C_i\frac{\partial u}{\partial x_i}=D\nabla^2 u+\frac{\partial G_i}{\partial x_i}+M \tag{13}$$

with β, C_i, D, G_i and M functions of time and location. Einstein summation notation is employed with $i=1,2$. The classical Garlekin FEM procedure is employed. One calculates integrals over each domain cell Ω_c using interpolation functions N_k, $(k=1\ldots n_d)$ as weighting functions:

$$\int_{\Omega_c}\beta N_k u\,d\Omega+\int_{\Omega_c}C_i N_k\frac{\partial u}{\partial x_i}d\Omega = \int_{\Omega_c}DN_k\nabla^2 u\,d\Omega+\int_{\Omega_c}N_k\frac{\partial G_i}{\partial x_i}d\Omega+\int_{\Omega_c}MN_k\,d\Omega. \tag{14}$$

After discretization, the resulting linear system of equations is solved by the BICGSTAB solver [30].

The numerical algorithm used is described in more detail in Ravnik et al. [22].

4. Shallow cavity

The solar thermal collector enclosed in a form of an open cavity is sketched in Fig. 1. The collector is partially bounded by fins – vertical walls which are 1/8 of the width of the collector. Considering the width of the collector to be 32 cm, the walls are $h=4$ cm high. The height h is considered to be the characteristic length scale of the problem and used to calculate Reynolds, Rayleigh and Nusselt numbers.

Air ($Pr=0.71$) of temperature $T_0=300$ K flows across the cavity. The bottom wall (the solar thermal collector) of the cavity is heated due to the absorption of the incoming irradiative heat from the sun. The process of absorption of heat radiation is not dealt with in the present study. In order to simplify the problem, an assumption is made that the bottom heated wall has a constant temperature. We assume a constant temperature along the bottom wall as $T_1=T_0+\Delta T$. The air enters the domain from the left having a uniform velocity profile of v_0. This velocity and the height of the cavity are used in definition of the Reynolds number.

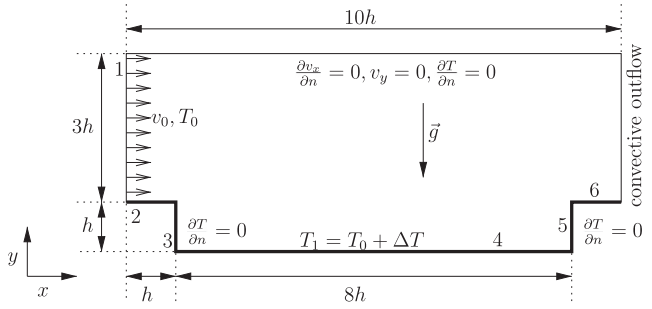

Fig. 1. Geometry and boundary conditions for flow over a shallow cavity. At inflow 1 uniform velocity profile is prescribed with constant temperature $\vec{v}=(v_0,0)$, $T=T_0$. No slip velocity boundary condition is used on solid walls 2–6. Walls 2 and 6 are kept at constant temperature T_0, walls 3 and 5 are adiabatic $\vec{\nabla}T\cdot\vec{n}=0$. Bottom wall 4 is kept at a constant temperature $T_1=T_0+\Delta T$. At outflow a convective [31,32] outflow boundary condition is used. Developed flow profile is assumed to be on the top wall $\vec{\nabla}T\cdot\vec{n}=0$ and $\vec{\nabla}v_x\cdot\vec{n}=0$, $v_y=0$.

Table 1
Reynolds and Rayleigh numbers for a shallow cavity having $h=0.04$ m, $T_0=300$ K, $\nu=16.1\times10^{-6}$ m^2/s, $\beta_T=1/T_0$, $\lambda=0.026198$ W/mK and Prandtl number $Pr=0.71$. Rayleigh number used in our simulations was $Ra=3\times10^5$, which corresponds to $\Delta T=52.6$ K and which makes $q_0=\lambda\Delta T/h=34.4$ W/m^2.

Re	v_0 (m/s)	$t_0=h/v_0$ (s)
5000	2.02	0.0198
10,000	4.03	0.0099
20,000	8.07	0.0049

The temperature difference between the bottom wall and incoming air, ΔT, is used in the Rayleigh number definition. Table 1 lists Reynolds and Rayleigh numbers and other non-dimensional parameters relevant for our simulations. Theoretically obtained Smagorinsky LES constant of $C=0.1$ and turbulent Prandtl number of $Pr_t=0.6$ were used.

The heat transfer through the bottom wall is represented by the Nusselt number Nu. The local Nusselt number is defined as the temperature gradient calculated at the wall. The average Nusselt number for the whole bottom wall is calculated by integration of the local Nu across the wall:

$$Nu=\frac{1}{8h}\int_0^{8h}\frac{\partial T}{\partial y}dx. \tag{15}$$

Heat flux is obtained by multiplying the Nusselt number and $q_0=\lambda\Delta T/h=34.4$ W/m^2.

Simulation were performed at $Ra=3\times10^5$, which corresponds to 52.6 K temperature difference between the air temperature at the inflow and the bottom wall temperature. Three inflow velocities were considered: $v_0=2.02$ m/s, 4.03 m/s, 8.07 m/s, which relate to Reynolds numbers $Re=5000$, $Re=10^4$ and $Re=2\times10^4$, respectively. At the lowest inflow air speed computational mesh *SC-25440* with 10^5 nodes was used. A finer mesh *SC-33900* with 1.36×10^5 nodes was used with 4.03 m/s inflow. At the highest inflow velocity, the fine mesh *SC-44900* with 2×10^5 nodes was employed. Details of the mesh structure are given in Table 2.

The vertical fins, which enclose the collector, help keep hot air above the collector and work towards decreasing heat losses. A collector without vertical fins can be modelled as a hot flat plate with cold air flowing over it. In order to compare results of the numerical simulation, we calculated heat losses of such a flat plate exposed to cold air flowing over it. Temperature difference and the flow velocity were the same as used in numerical experiments. We assume that the solar collector is mounted on a roof, thus a turbulent boundary layer develops already before the flow reaches the flat plate collector. Based on the boundary layer theory, the following expression can be used to calculate the heat flux from the flat plate:

$$q_{fp}=\alpha\Delta T,\quad \alpha=2\frac{\lambda}{8h}0.037\left(\frac{v_0 8h}{\nu}\right)^{0.8}Pr^{1/3}. \tag{16}$$

4.1. $Re=5000, Ra=3\times10^5$

Simulation was performed using a time step of $\Delta t=10^{-2}$ without a subgrid model. Total number of time steps was 12,500 which relates to 2.475 s in our chosen geometrical setup. Structures in the flow are large enough that our mesh is able to describe them all. When flow enters the cavity vortical structures are formed behind the edge of the cavity. Structures are similar to the well known backward facing step flow. A primary vortex develops behind the cavity wall. Since in the case of solar collectors the length of the collector is much larger than the height of the cavity, the primary vortex does not encompass the entire collector. Instead, we observe vortex shedding. Vortices are

Table 2
Computational grids used to simulate flow over a shallow cavity. Nine-nodal Lagrange quadratic internal cells and three-nodal boundary elements were used.

Mesh	No. elements along edges					No. boundary elements	No. internal cells	Total no. nodes
	1	2	3	4	6			
SC-25440	40	12	40	300	24	832	25,440	102,593
SC-33900	40	12	50	350	48	1000	33,900	136,601
SC-49900	50	24	63	400	70	1214	49,900	200,813

lifted into the flow and transported by convection across the domain. On the right-hand side of the domain we also observe formation of vortices, which are carried by the flow across the sharp cavity edge out of the domain. Furthermore, behind the sharp edge a large number of smaller vortices are observed. Those are immediately convected out of the domain and do not affect the heat transfer from the bottom wall.

Fig. 2 shows temperature contours for three time instants. In the same figure, a graph of the Nusselt number across the bottom wall is displayed. We can observe high heat transfer (and hence high Nusselt number) in areas of the bottom wall where temperature gradients are high. Such areas move along the wall as the flow carries the vortices across the domain.

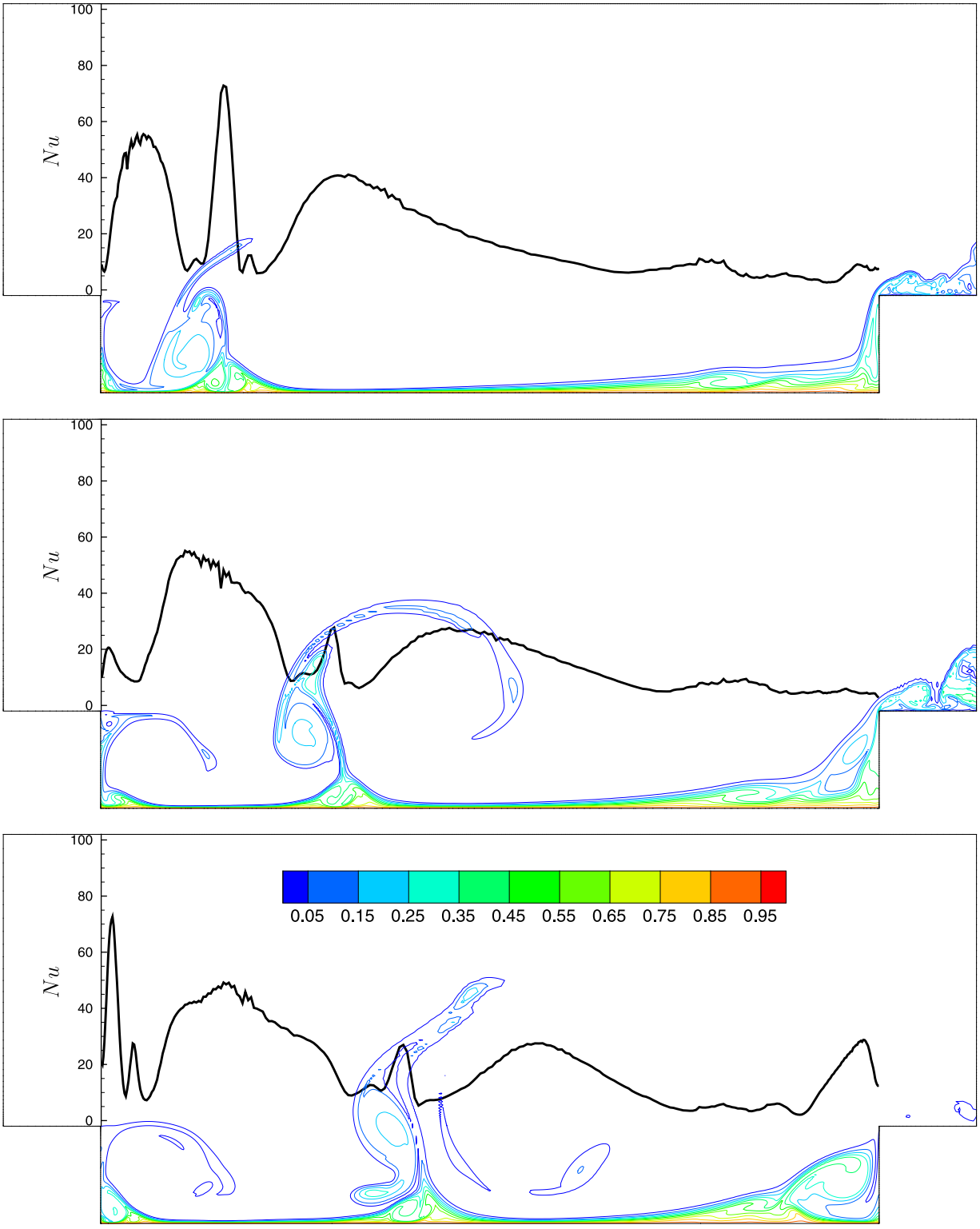

Fig. 2. Nondimensional temperature contours and Nusselt number along the bottom wall for $Re = 5000, Ra = 3 \times 10^5$. Three time instants were chosen, which show the formation and shedding of a vortex. There were 1200 time steps between the time instants, which relate to $1200 \times 10^{-2} \times 0.0198\ \mathrm{s} = 0.24\ \mathrm{s}$.

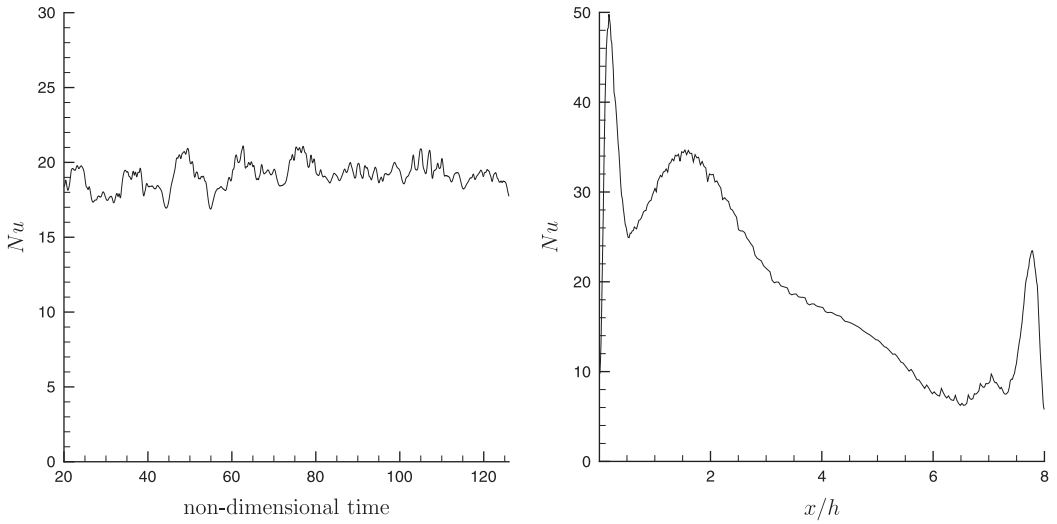

Fig. 3. Average Nusselt number across the bottom wall (right); time trace of averaged Nusselt number (left) $Re = 5000, Ra = 3 \times 10^5$. No subgrid model was used.

Table 3
Time averaged heat transfer – expressed with Nusselt number and heat flux $q = Nu \cdot q_0$. We present a comparison between simulation without a subgrid model ($C=0$) and simulation with Smagorinsky subgrid model with Van Driest damping along solid walls LES_{vd}. Boundary layer theory based value for a flat plate collector is also presented for comparison.

v (m/s)	$C=0$		LES_{vd}		Flat plate (Eq. (16))
	Nu	q (W/m^2)	Nu	q (W/m^2)	q_{fp} (W/m^2)
2.02	19.2	220.4			1369
4.03	30.2	1039	29.9	1029	2380
8.07	45.5	2611	35.4	2031	4147

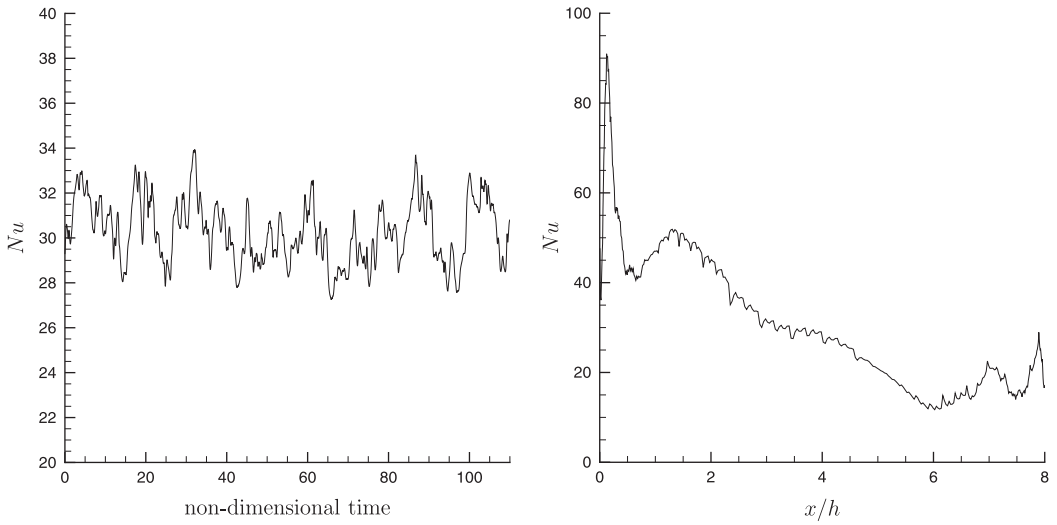

Fig. 4. Average Nusselt number across the bottom wall (right); time trace of averaged Nusselt number (left) $Re = 10^4, Ra = 3 \times 10^5$. No subgrid model was used.

Fig. 3 displays the time averaged Nusselt number across the bottom wall of the cavity (across the solar collector). We observe that the heat transfer is the largest on the left hand side, behind the cavity wall, and the smallest in the central part of the cavity. Another peak in heat transfer is observed on the right hand side, just before the cavity wall. In the same figure, time trace of Nusselt number averaged across the bottom wall is presented. We see that the heat transfer periodically oscillates and does not deviate much from the average value. Time averaged value is given in Table 3. Comparing the heat losses of the enclosed collector with the flat plate model, we observe that the vertical fins significantly reduce the heat transfer.

4.2. $Re = 10^4, Ra = 3 \times 10^5$

Next we increased the inflow air velocity by a factor of two, thus effectively raising the Reynolds number to $Re = 10^4$. Correspondingly we decreased the time step to $\Delta t = 5 \times 10^{-3}$. Simulation was performed without a subgrid model and with a Smagorinsky subgrid model with Van Driest damping. Without

the subgrid model simulation had 11,000 time steps lasting for 0.544 s, with the subgrid model the number of time steps was 16,000 and the total time was 0.792 s.

Comparison of time averaged heat transfer (shown in Table 3) reveals that the use of the subgrid model in this case has negligible effect on the average heat transfer. Both simulations predict the same average Nusselt number. In comparison with the flat plate collector, we observe that the heat losses of the enclosed collector are about one-half of the losses of a collector, which does not have vertical fins.

Time traces of the Nusselt number and its time average across the bottom wall are shown for both simulations in Figs. 4 and 5. Similar to the low Reynolds number case described above, the highest heat transfer occurs behind the left cavity wall. Looking at the time traces we observe that Nusselt number oscillations include higher frequencies, which indicates the presence of small scale structures in the flow field.

4.3. $Re = 2 \times 10^4, Ra = 3 \times 10^5$

Finally, the inflow velocity was increased to 8.07 m/s corresponding to $Re = 2 \times 10^4$. Time step of $\Delta t = 10^{-3}$ was used. Simulation without a subgrid model lasted for 0.3 s having 60,000 time steps. Simulation with subgrid model was run for 0.1 s having 20,000 time steps.

Fig. 6 shows vorticity contours and streamlines for one time instant. One readily observes the formation of vortices along the whole length of the bottom wall. Time traces and time averaged Nusselt numbers are shown in Figs. 7 and 8 as well as in Table 3.

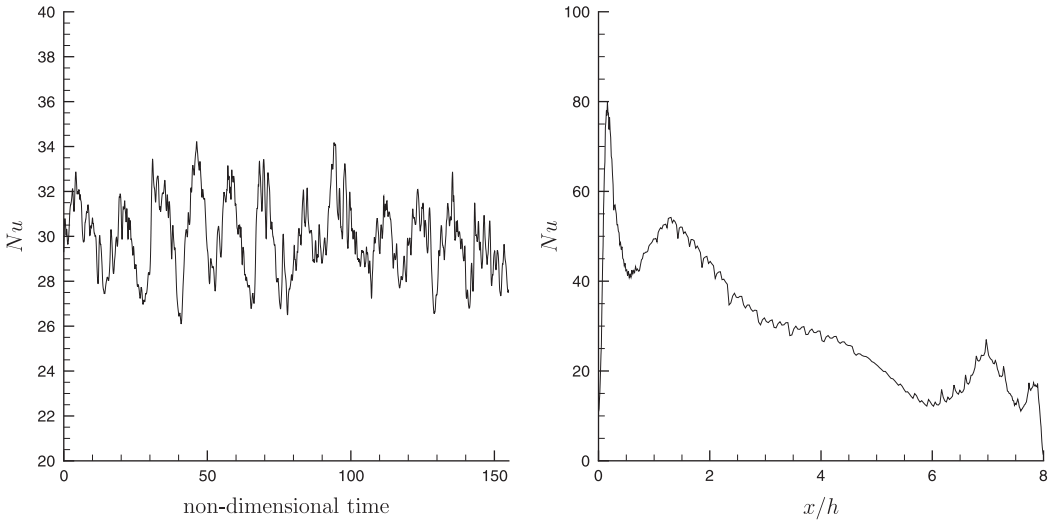

Fig. 5. Average Nusselt number across the bottom wall (right); time trace of averaged Nusselt number (left) $Re = 10^4, Ra = 3 \times 10^5$. Smagorinsky subgrid model was used with Van Driest damping.

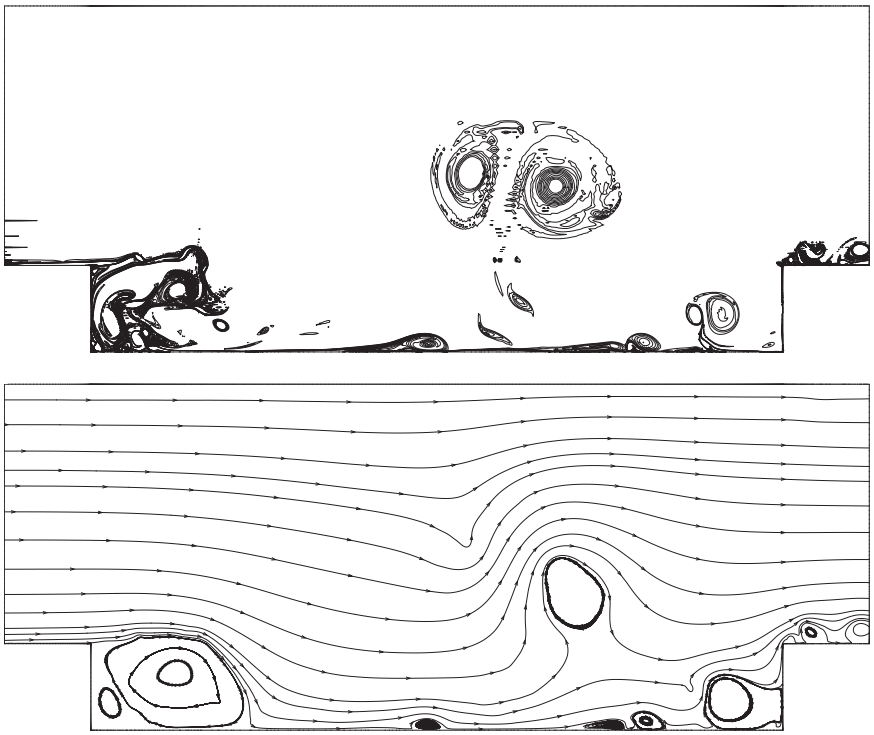

Fig. 6. Vorticity contours (top) and streamlines (bottom) for $Re = 2 \times 10^4, Ra = 3 \times 10^5$. Smagorinsky subgrid model with Van Driest damping is used.

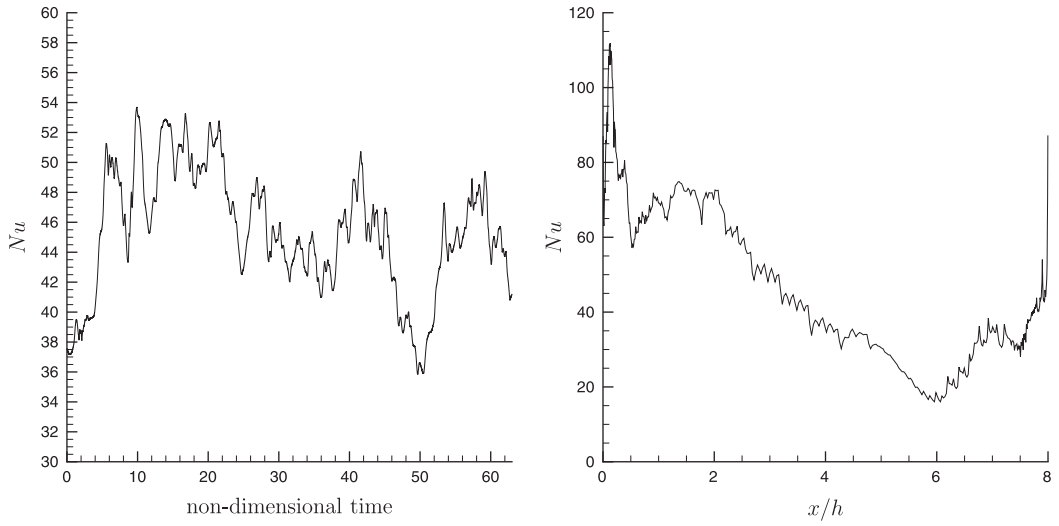

Fig. 7. Average Nusselt number across the bottom wall (right); time trace of averaged Nusselt number (left) $Re = 10^4, Ra = 3 \cdot 10^5$. No subgrid model was used.

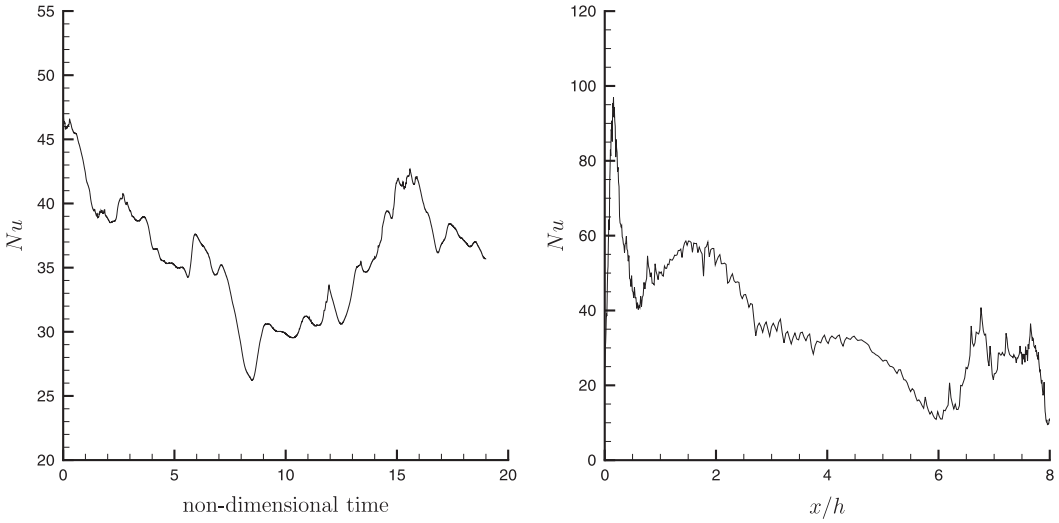

Fig. 8. Average Nusselt number across the bottom wall (right); time trace of averaged Nusselt number (left) $Re = 2 \times 10^4, Ra = 3 \times 10^5$. Smagorinsky subgrid model was used with Van Driest damping.

We observe a high difference in heat transfer for both simulations. Simulation without the subgrid model reports higher values of heat transfer. In comparison with RANS simulation, performed by Zdanski et al. [4], we can confirm that our simulation using the subgrid model gives a better prediction of the heat transfer.

In comparison with the flat plate collector, we observe that the heat losses of the enclosed collector are about one-half of the losses of a flat plate collector.

5. Conclusions

The coupled boundary element–finite element algorithm for planar velocity–vorticity LES was used to simulate flow and heat transfer from a solar thermal collector. The collector was enclosed by fins creating an open shallow cavity for air flowing over it. Heat transfer from the bottom wall of the cavity (the collector) was studied for different air flow velocities. Unsteady LES simulations were performed having up to 60,000 time steps.

We presented time traces of average Nusselt number as well as averaged Nusselt number along the bottom wall. We have found that the highest heat flux from the collector can be in all cases found behind the vertical fin. Heat flux there is up to three times higher than in the central part of the collector. The reason for this phenomenon is the shedding of large vortices behind the fin, which effectively carry the hot air away from the collector.

Looking at the time evolution of the heat flux in self-similar flow regime we observe heat flux oscillations of about $\pm 10\%$ in the case of $Re \leq 10^4$ and of about $\pm 20\%$ at $Re = 2 \times 10^4$

Comparison of simulations with and without the subgrid scale model was made. Results were equivalent for low Reynolds number, while at higher Re simulation without subgrid scale model over predicted the heat transfer.

When average heat losses of an enclosed collector are compared with a flat plate collector, one observes that the flat plate collector heat losses are significantly larger. At low wind speed the ratio of heat loss of a flat plate collector and enclosed collector is about five. At higher speeds the ratio drops to about two. These are important conclusions when considering engineering design of solar collectors, as the use of empirical correlations, valid for only partially similar geometries, leads to unrealistic values of design parameters, in our case heat losses to the surroundings. Applying an advanced turbulence modelling technique – the LES – enables realistic determination of complex recirculating flow field inside

the cavity, the key factor in accurate prediction of turbulent heat transfer from the solar collector.

References

[1] Gomes DG. Optimization of flat plate solar collectors [Master's thesis]. São José dos Campos, Brazil: TIA—Technological Institute of Aeronautics; 1998.
[2] Zdanski PSB, Ortega MA, Fico N. Convection effects in flows over cavities of high aspect ratios. AIAA Pap 2002:3301.
[3] Zdanski PSB, Ortega MA, Fico N. Numerical study of the flow over shallow cavities. Comput Fluids 2003;32:953–74.
[4] Zdanski PSB, Ortega MA, Fico NGCR. Heat transfer studies in the flow over shallow cavities. J Heat Transf 2005;127:699–712.
[5] Vardoulakis S, Fisher BEA, Pericleous K, Gonzales-Flesca N. Modelling air quality in street canyons: a review. Atmos Environ 2003;37:155–82.
[6] Penot F. Numerical calculation of two-dimensional natural convection in isothermal open cavities. Numer Heat Transf 1982;5:421–37.
[7] Chan Y, Tien C. A numerical study of two-dimensional natural convection in square open cavities. Numer Heat Transf 1985;8:65–80.
[8] Chan Y, Tien C. Laminar natural convection in shallow open cavities. J Heat Transf 1986;108:305–9.
[9] Bilgen E. Passive solar massive wall systems with fins attached on the heated wall and without glazing. J Solar Energy Eng 2000;122:30–4.
[10] Mesalhy O, Aziz S, El-Sayed M. Flow and heat transfer over shallow cavities. Int J Therm Sci 2010;49:514–21.
[11] Polat O, Bilgen E. Conjugate heat transfer in inclined open shallow cavities. Int J Heat Mass Transf 2003;46:1563–73.
[12] Alloui Z, Vasseura P. Natural convection in a shallow cavity filled with a micropolar fluid. Int J Heat Mass Transf 2010;53:2750–9.
[13] Alloui Z, Vasseur P, Reggio M. Natural convection of nanofluids in a shallow cavity heated from below. Int J Therm Sci 2011;50:385–93.
[14] Salat J, Xin S, Joubert P, Sergent A, Penot F, Quéré PL. Experimental and numerical investigation of turbulent natural convection in a large air-filled cavity. Int J Heat Fluid Flow 2004;25:824–32.
[15] Peng SH, Davidson L. Large eddy simulation for turbulent buoyant flow in a confined cavity. Int J Heat Fluid Flow 2001;22:323–31.
[16] Tenaud C, Pellerin S, Dulieu A, Phuoc LT. Large eddy simulation of a spatially developing incompressible 3D mixing layer using v–ω formulation. Comput Fluids 2005;34:67–96.
[17] Mansfield JR, Knio OM, Meneveau C. A dynamic LES scheme for vorticity transport equation: formulation and a priori tests. J Comput Phys 1998;145:693–730.
[18] Škerget L, Hriberšek M, Kuhn G. Computational fluid dynamics by boundary domain integral method. Int J Num Methods Eng 1999;46:1291–311.
[19] Ramšak M, Škerget L. A subdomain boundary element method for high-Reynolds laminar flow using stream function - vorticity formulation. Int J Numer Methods Fluids 2004;46:815–47.
[20] Žunič Z, Škerget L, Hriberšek M, Ravnik J. Boundary element-finite element method for velocity–vorticity formulation of Navier–Stokes equations. In: WIT transactions on modelling and simulation, vol. 41, 2005. p. 793–802.
[21] Ravnik J, Škerget L, Hriberšek M. The wavelet transform for BEM computational fluid dynamics. Eng Anal Bound Elem 2004;28:1303–14.
[22] Ravnik J, Škerget L, Hriberšek M. 2D velocity vorticity based LES for the solution of natural convection in a differentially heated enclosure by wavelet transform based BEM and FEM. Eng Anal Bound Elem 2006;30:671–86.
[23] Pope S. Turbulent flows. Cambridge: Cambridge University Press; 2000.
[24] Sagaut P. Large eddy simulation for incompressible flows, an introduction. Berlin, Heidelberg, New York: Springer Verlag; 2002.
[25] Taylor GI. The transport of vorticity and heat through fluids in turbulent motion. Proc R Soc London Ser A 1932;135:685–705.
[26] Smagorinsky J. General circulation experiments with the primitive equations: I. the basic equations. Mon Weather Rev 1963;91:99–164.
[27] Mansour NN, Ferziger JH, Reynolds WC. Large-eddy simulation of a turbulent mixing layer, Report TF-11, Thermosciences Div., Department of Mechanical Engineering, Standford University, 1978.
[28] Winckelmans GS, Lund TS, Carati D, Wray AA. A priori testing of subgrid-scale models for the velocity pressure and vorticity–velocity formulations. In: Proceedings of the summer program, center for turbulence research, 1996.
[29] Breuer M. Direkte Numerische Simulation und Large-Eddy Simulation turbulenter Strömungen auf Hochleistungsrechnern. Aachen: Shaker Verlag; 2002.
[30] Sleijpen GLG, Fokkema DR. BICGSTAB for linear equations involving unsymmetric matrices with complex spectrum. Electron Trans Numer Anal 1993;1:11–32.
[31] Orlanski I. A simple boundary condition for unbounded hyperbolic flows. J Comput Phys 1976;21:251–69.
[32] Kobayashi M, Periera J, Sousa J. Comparison of several open boundary numerical treatments for laminar recirculating flows. Int J Numer Methods Fluids 1993;16:403–19.